RSC Advances

PAPER

View Article Online
View Journal | View Issue

Cite this: *RSC Adv.*, 2026, **16**, 12132

Carbon dots derived from *Averrhoa bilimbi* fruit for the detection of cholesterol and chromium(VI)

Aishwarya Joji Mathew,[a] Varsha Lisa John,[a] P. S. Aiswarya[a] and T. P. Vinod *[ab]

Received 9th January 2026
Accepted 23rd February 2026

DOI: 10.1039/d6ra00222f

rsc.li/rsc-advances

Carbon dots (CDs) are a class of carbon-based nanomaterials, typically less than 10 nm in size, known for their unique optical and electronic properties. Their discovery led to the opening of new avenues in nanotechnology, particularly in the field of fluorescence-based sensing. Owing to their strong photoluminescence, excellent aqueous solubility, low cytotoxicity, and potential surface functionalization, CDs have been considered as effective fluorescent probes for the detection of a wide range of analytes. Herein, we report the hydrothermal synthesis of CDs from a natural source, *Averrhoa bilimbi* fruit, leading to the formation of CDs exhibiting useful photoluminescent properties and potential for selective detection of cholesterol and Cr(VI) ions. The average particle size of *Averrhoa bilimbi* fruit-derived CDs (AB-CDs) was found to be 6.022 nm. The properties of AB-CDs were unravelled from structural and optical characterization and the applicability of AB-CDs as sensors for heavy metals and biomarkers was studied. The selective fluorescence response towards cholesterol and Cr(VI) makes it an efficient fluoroprobe for practical applications. The limits of detection for the sensing of cholesterol and Cr(VI) were estimated to be 0.31 μM and 1.71 μM respectively. The sensor system using AB-CDs is economical, sustainable, and eco-friendly.

1. Introduction

Carbon dots (CDs) are zero dimensional, fluorescent nanomaterials with quasi-spherical structure, exhibiting sizes ranging between 1–10 nm.[1] CDs were accidently discovered in 2004 during the electrophoretic purification of single walled carbon nanotubes (SWCNTs).[2] CDs are water-soluble nanoparticles consisting of a graphitic core surrounded with functional groups such as –OH, –COOH, $–NH_2$, or H atoms. CDs have attracted interest as fluorescent sensors because of their unique optical behaviour, high biocompatibility, and facile surface modification.[3,4] Employing CDs for fluorescence sensing applications holds great promise as they can be prepared from cheaper sources, and the detection of analytes using CDs is generally rapid and cost-effective.[5–9] CDs can be synthesized from both natural and synthetic sources. CDs prepared from natural sources have gained popularity as they follow a green approach based on sustainability, cost-effectiveness, and easy access to precursors.[10] In this study, we report a green, facile, and straightforward one-pot hydrothermal synthesis of CDs from *Averrhoa bilimbi*. *Averrhoa bilimbi*, commonly known as *bilimbi,* belongs to the *Oxalidaceae* family, and is widely grown in tropical regions for its nutritionally rich fruits. *Bilimbi* fruit serves as an eco-friendly, cost-effective, and sustainable precursor, enabling the green synthesis of highly fluorescent, water-soluble CDs suitable for sensing applications. Usage of *Averrhoa bilimbi* as a precursor of CDs for the multi analyte sensing of Cr(VI) and cholesterol has not been reported to date.

Heavy metal pollution poses a serious global environmental threat, primarily due to the release of inorganic industrial effluents into aquatic systems.[11] Among these, Cr(VI) is of particular concern because of its high toxicity, carcinogenicity, and environmental persistence.[12] Cr(VI) readily penetrates biological membranes, inducing oxidative stress and DNA damage, which can lead to severe health disorders.[13] Consequently, the sensitive and selective detection of Cr(VI) is essential for effective environmental monitoring. Traditional analytical methods, including chromatographic methods like gas chromatography, high-performance liquid chromatography, inductively coupled plasma optical emission spectrometry (ICP-OES), inductively coupled plasma mass spectrometry (ICP-MS) and atomic absorption spectroscopy (AAS), have been widely used for heavy metal ions detection.[14] However, these methods have several limitations, such as high instrument costs, complex sample preparation, lack of portability, and the need for trained personnel.[15] Considerable efforts have been dedicated to develop cost-effective and selective fluorescent sensors for detecting heavy metals, as the fluorometric approach offers several advantages, including high sensitivity, fast response, and low cost.[16] Cholesterol plays a vital role in physiological

[a]*Department of Chemistry, Christ University, Hosur Road, Bengaluru 560029, India. E-mail: vinod.tp@christuniversity.in*

[b]*Centre for Renewable Energy and Environmental Sustainability, Christ University, Bengaluru 560029, India*

processes such as hormone synthesis, vitamin D production, and maintenance of cell membrane integrity.[17] However, elevated levels of low-density lipoprotein (LDL) cholesterol, commonly referred to as "bad cholesterol," are associated with adverse health effects, including impaired blood flow, arterial plaque formation, peripheral artery disease, and an increased risk of stroke and cardiovascular disorders.[18] Detection of cholesterol using the conventional techniques possess many limitations, due to which the rapid and selective detection of cholesterol is essential. Therefore, the need for fluorescence sensing of biomolecules arises from the demand for rapid, specific, sensitive, cost effective, user-friendly, and real-time detection.

We report the synthesis of *Averrhoa bilimbi* fruit-derived CDs (AB-CDs), which exhibited multi-analyte sensing capability by selectively detecting both Cr(VI) ions and cholesterol. Owing to its sustainable, renewable, eco-friendly, cost-effective, and biocompatible nature, AB-CDs can serve as an efficient and low-cost fluorescent probe for the sensitive detection of Cr(VI) ions and cholesterol.

2. Materials and methods

2.1 Chemicals

Averrhoa bilimbi fruit was acquired from Kochi, India, and stored at 4 °C. $K_2Cr_2O_7$, quinine sulphate (QS), $AlCl_3$, As_2O_3, $CdCl_2$, $CuSO_4$, $ZnCl_2$, $CaCl_2$, $FeCl_2$, NaCl, $PbCl_2$, $HgCl_2$, $FeCl_3$, KCl, $Na_2HPO_4 \cdot 12H_2O$, NaH_2PO_4, ascorbic Acid (AA), dopamine (DA), cholesterol, D-glucose, creatinine, L-glycine, L-lycine, thiamine, L-tryptophan, and L-tyrosine were purchased from Prince Chemicals. Acetone and ethanol were purchased from Future lab. Syringe filters with a 0.22 μm pore size, dialysis membrane-70 with a molecular weight cutoff ranging from 12 000 Da to 14 000 Da were sourced from science world, Bangalore, India.

2.2 Synthesis of AB-CDs

The collected samples of *Averrhoa bilimbi* fruit was washed thoroughly to remove impurities. The cleaned fruits were churned in a blender to obtain its juice. 80 ml of the juice was transferred to a 100 ml Teflon-lined hydrothermal autoclave and heated to 180 °C for 12 hours to obtain a brown-coloured suspension. This suspension was filtered using syringe filter and dialyzed for 48 hours to obtain purified AB-CDs (with the concentration of 0.505 mg ml^{-1}).

2.3 Preparation of AB-CDs samples for XRD and Raman analysis

The aqueous dispersions of AB-CDs were drop-cast onto a clean glass slide and allowed to dry, forming a uniform thin film. After complete solvent evaporation, the coated glass slide was mounted in the XRD sample holder, and diffraction patterns were recorded over a 10–90° 2θ range. Similarly, the coated glass slide was analysed by Raman spectroscopy using an appropriate laser radiation (514 nm from an Ar^+ laser).

2.4 Characterization

pHep + waterproof pocket pH tester (0.01 pH Resolution-HI98108) was used to check the pH of solutions used for the experiments. Fourier Transform Infrared (FTIR) spectroscopy of AB-CDs was performed on a PerkinElmer Spectrum 100 series spectrometer, operating over 4000–500 cm^{-1}. XPS analysis was performed using a PHI Model 5802, and the Raman spectrum of AB-CDs (4000–100 cm^{-1}) was recorded with an INVIA Raman spectrometer (514 nm Ar^+ laser, UK). XRD analysis was conducted using a Bruker D8 Advance diffractometer (Cu-Kα, λ = 1.5406 Å, 40 kV, 20 mA, 10–90° 2θ), and HRTEM images were obtained on a JEOL JEM-2100 (LaB_6, 200 kV). Particle size and zeta potential were determined using Dynamic Light Scattering (DLS) on a Zetasizer (ZS90) instrument. UV-visible absorbance of AB-CDs was recorded using a Shimadzu UV-1500 spectrophotometer, while photoluminescence and excitation spectra were measured with a Shimadzu RF-5301 spectrofluorometer. PL decay measurements were performed using a JOBIN-YVON Fluorocube lifetime system.

2.5 Detection of Cr(VI) and cholesterol

For Cr(VI) ion detection, 0.3 ml of aqueous AB-CDs dispersion was mixed with 2.5 mL of pH 7 phosphate buffer solution (PBS), followed by the addition of varying volumes of 1 mM Cr(VI) solution. After incubating for 10 min at room temperature, PL spectra of the solution were recorded using fluorescence spectrophotometer using an excitation at 320 nm. The detection of cholesterol was also carried out using the same protocol.

2.6 Determination of quantum yield (QY)

The QY of AB-CDs was calculated using eqn (1), where 'st' refers to the reference standard (QS), and 'x' represents the AB-CDs. The QY of QS, used as the standard in 0.1 M H_2SO_4, is known to be 54%. In eqn (1), η denotes the refractive index of water as solvent, A is the absorbance, Q is the quantum yield, and I correspond to the PL intensity, measured when excited at the wavelength of 320 nm.

$$Q_x = Q_{st} \times \frac{A_{st}}{A_x} \times \frac{I_x}{I_{st}} \times \left(\frac{\eta_x^2}{\eta_{st}^2}\right) \quad (1)$$

2.7 Limit of detection

The limit of detection (LOD) for Cr(VI) and cholesterol was calculated using eqn (2).[19]

$$\mathrm{LOD} = \frac{3\sigma}{S} \quad (2)$$

where σ represent standard deviation and S represent slope of the plot of PL intensity against the concentrations of Cr(VI) and cholesterol, respectively.

3. Results and discussion

Bilimbi fruit was employed as a sustainable, cost-effective (~110 Indian rupees per Kg), and eco-friendly precursor for the

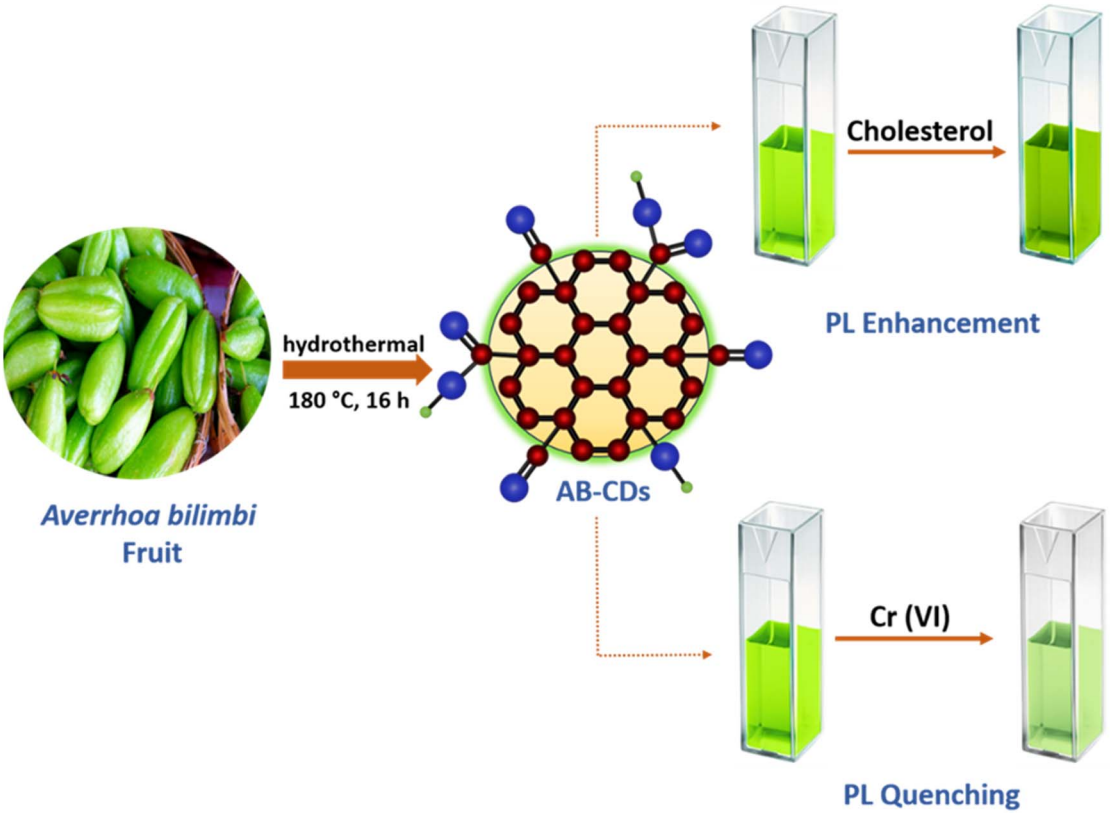

Fig. 1 Schematic representation of the synthesis of AB-CDs for the selective detection of cholesterol and Cr(VI).

hydrothermal synthesis of AB-CDs. AB-CDs were subsequently purified using syringe filtration followed by dialysis. The purity of the AB-CDs was evaluated following the dialysis process. The PL responses of both the retentate and dialysate were recorded after 24 h of dialysis. As shown in Fig. S1 (SI), the retentate exhibits a significantly higher PL intensity than the dialysate, confirming that the major fluorescent product is the AB-CDs. The weak PL responses observed for the dialysate are presumed to be from small amount of fluorescent byproducts, which were effectively removed during dialysis. Also, it is possible that a small number of CDs entered the dialysate through the tied-up ends of the dialysis bag. AB-CDs were characterized to analyse their structural and optical features, confirming their formation. Furthermore, AB-CDs acts as a fluoroprobe for the sensing of both Cr(VI) and cholesterol (Fig. 1).

3.1 Structural characterizations of AB-CDs

The morphology and the size of the AB-CDs were studied using high resolution transmission electron microscopy (HRTEM).

HRTEM analysis revealed that AB-CDs possess a quasi-spherical morphology (Fig. 2a). The size distribution histogram indicated that AB-CDs had mean particle diameter of 6.022 nm (Fig. 2b). Lattice spacing of 0.22 nm were observed for AB-CDs in HRTEM analysis, which indicates characteristic of (100) plane of graphitic carbon (Fig. 2c).

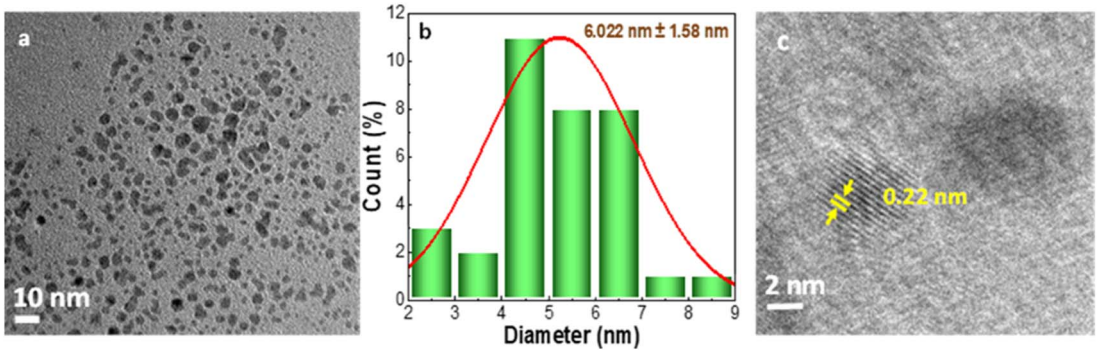

Fig. 2 (a) TEM image, (b) size distribution histogram, and (c) HRTEM image of AB-CDs respectively.

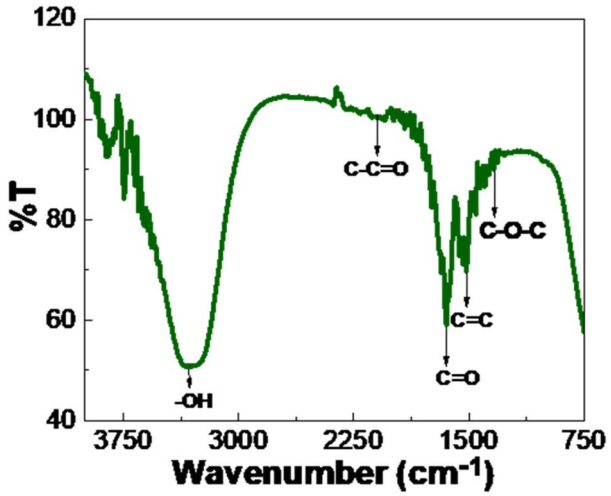

Fig. 3 FTIR spectrum of AB-CDs.

FTIR spectroscopy was used to identify the functional groups on the surface of AB-CDs. FTIR spectrum revealed characteristic bands at 3328.6 cm^{-1} corresponding to –OH stretching, 2089.7 cm^{-1} attributed to C–C=O stretching, 1510.2 cm^{-1} associated with C=C stretching, and 1333.9 cm^{-1} corresponding to C–O–C stretching. Additionally, the band at 1648.8 cm^{-1} indicated the presence of C=O functional groups, confirming the abundance of alcohol and carbonyl-rich functional groups on the surface of AB-CDs (Fig. 3). Additionally, –COOH and C=O groups may contribute to the long-range fluorescence observed in AB-CDs, while peak broadening could result from hydrogen-bonding interactions.[20,21] AB-CDs were highly hydrophilic and showed excellent water dispersibility, due to surface polar functionalities. The surface charge of AB-CDs was found to be 24.8 mV from the zeta potential measurement (Fig. S2a, SI). This negative zeta potential value confirms that the surface of AB-CDs consists of alcoholic and carbonyl functional groups, leading to good colloidal stability.

XPS analysis was performed to further investigate the presence of functional groups on AB-CDs. The XPS analysis was

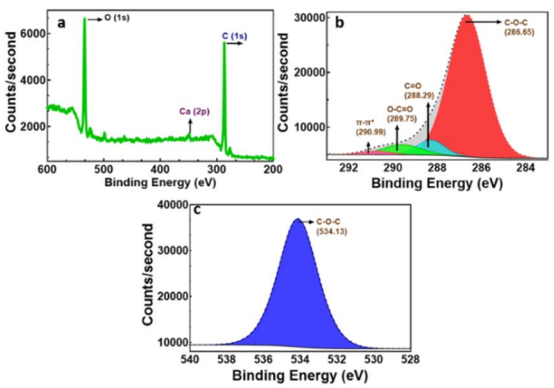

Fig. 4 (a) XPS Survey spectrum of AB-CDs, and (b and c) deconvoluted XPS spectra in the C 1s, and O 1s regions, recorded from the AB-CDs respectively.

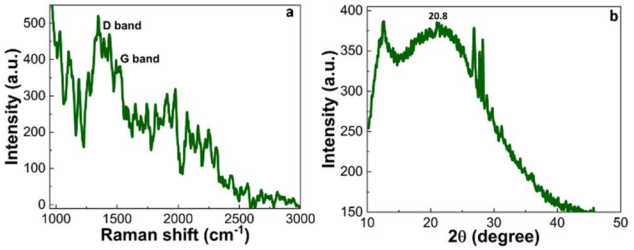

Fig. 5 (a) The Raman spectrum, and (b) XRD spectrum of AB-CDs respectively.

conducted to study the elemental composition of the AB-CDs. XPS survey spectrum indicated the presence of O 1s, Ca 2p, and C 1s peaks (Fig. 4a). The C 1s deconvoluted spectra indicated peaks at 290.99 eV associated with C sp^2, 286.65 eV corresponding to C–O–C, 289.75 eV due to O–C=O and C=O at 288.29 eV (Fig. 4b). O 1s deconvoluted spectra showed peaks equivalent to C–O–C (534.13 eV) functional group (Fig. 4c). The presence of C and O on the surface of AB-CDs is ascertained through XPS analysis.

Raman spectroscopy was utilized to study the degree of disorder, graphitic content, and degree of defects in AB-CDs. The Raman spectrum shown in Fig. 5a features two peaks at 1373.64 cm^{-1} and 1543.33 cm^{-1}. The D band observed at 1373.64 cm^{-1} corresponds to the A_{1g} breathing mode and reflects structural defects near the *K* points of the first Brillouin zone. In contrast, the G band at 1543.33 cm^{-1} is associated with sp^2-hybridized carbon clusters and originates from the E_{2g} phonon mode. These Raman shifts, representing the first-order D and G peaks, provide insight into the defect density, structural disorder, and crystallinity of the AB-CDs.[22] The crystallographic structure of AB-CDs was examined through XRD. The low intensity band observed at 20.8° in the XRD indicates the (002) facet of graphite. AB-CDs exhibited an amorphous nature shown by the low intensity and broader full-width at half maximum in the XRD spectra. The broad peak further suggests incomplete graphitization and nanoscale dimensions of AB-CDs (Fig. 5b).[23] The *d*-spacing of AB-CDs was estimated to be 0.42 nm from XRD spectra using Bragg's law.

3.2 Optical characterizations of AB-CDs

The optical characteristics of AB-CDs are presented in Fig. 6. UV-visible absorption spectroscopy of AB-CDs was employed to examine its electronic transition behaviour. The absorbance peaks around 298 nm and 245 nm in AB-CDs corresponds to n–π* transition (C=O bonds) and π–π* transitions (C=C bonds) (Fig. 6a). These electronic transitions occur within the graphitic domains and defect sites on the surface of CDs. The absorption tail extending into longer wavelength regions may result from multiple low-energy transitions caused by the functional groups present on the surface of CDs.[24] A broad absorption band is seen in the absorption spectrum, likely resulting from the size and surface heterogeneity of AB-CDs.[25] AB-CDs showed maximum emission at 380 nm upon excitation at 320 nm radiation (Fig. 6b). AB-CDs exhibited excitation dependent fluorescence

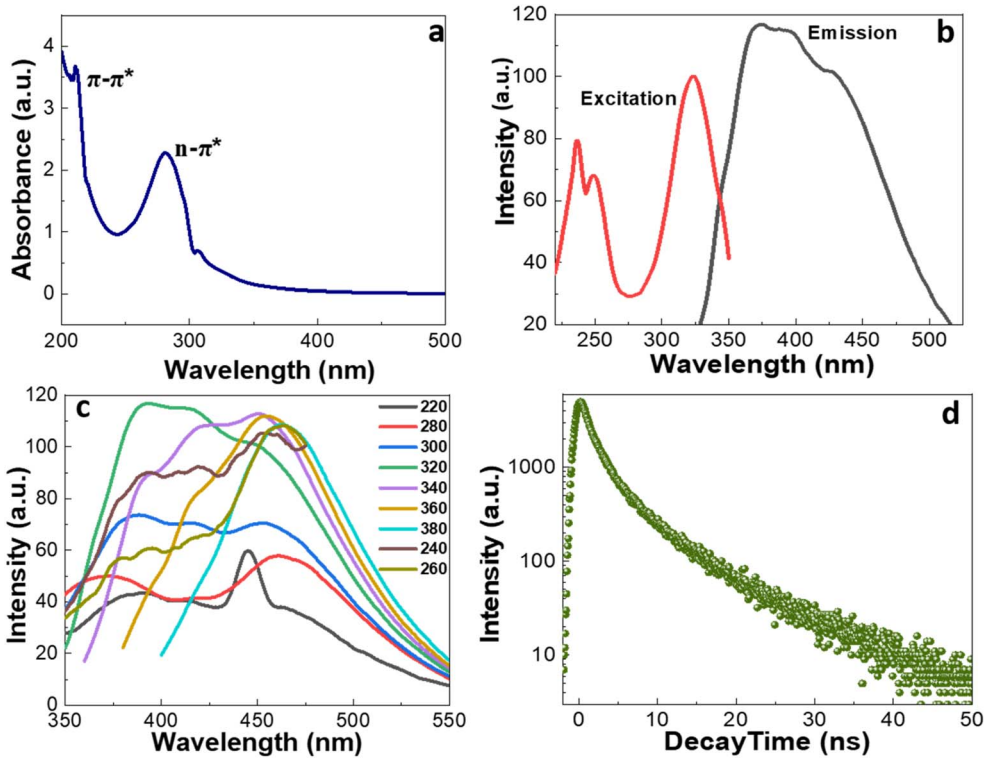

Fig. 6 (a) Absorption spectrum of AB-CDs recorded using UV-visible spectroscopy, (b) excitation spectrum (emission monitored at 380 nm) and emission spectrum ($\lambda_{ex} = 320$ nm) of AB-CDs, (c) excitation wavelength dependent PL emission spectra of AB-CDs, and (d) fluorescence lifetime spectrum of AB-CDs.

when excited across wavelengths from 220 to 380 nm (Fig. 6c). The surface defects, electronegativity of heteroatoms, and synergistic models have been proposed to explain the excitation-dependent photoluminescence observed in CDs.[26] The QY of AB-CDs was calculated to be 1.62%. The estimated fluorescence lifetime of AB-CDs was about 4.3 ns by fitting the decay curve using multi-exponential function of the lifetimes of $\tau_1 = 2.05$ ns (35%), $\tau_2 = 2.05$ ns (41%), $\tau_3 = 6.94$ ns (24%) (Fig. 6d).

The pH-dependent behaviour on PL emission of AB-CDs is clearly shown in Fig. 7a. Upon examining the effect of pH on the photoluminescence of AB-CDs, a noticeable quenching of fluorescence is observed under acidic conditions, as shown in Fig. 7b. The fluorescence quenching observed between pH 7 and 11 is relatively negligible. The slight pH sensitivity of AB-CDs can be attributed to electronic transitions associated with defect states. Excess hydrogen and hydroxyl ions may disrupt these defect sites, leading to alterations in surface functional groups and consequent fluorescence quenching.[27] The photostability of AB-CDs was studied and is shown Fig. 7c. AB-CDs exhibit a decline in PL intensity, showing only a 2.54% decrease in PL intensity after one month of storage and a 4.66% reduction after six months of storage. This reduction in photostability is attributed to the aggregation behaviour of AB-CDs.

Further, the stability of AB-CDs towards temperature and KCl concentration was studied, and the results are presented in Fig. S2 (SI). Fig. S2a, SI, shows the effect of ionic strength on the PL intensity of AB-CDs. A pronounced decrease in PL intensity is observed with increasing KCl concentration, which can be attributed to the aggregation of particles, which is induced by the higher salt content.[28] AB-CDs exhibited excellent thermal stability when the temperature was varied from 30 to 90 °C (Fig. S2b, SI). The fluorescence intensity remained nearly constant across this range, indicating that the carbon core and

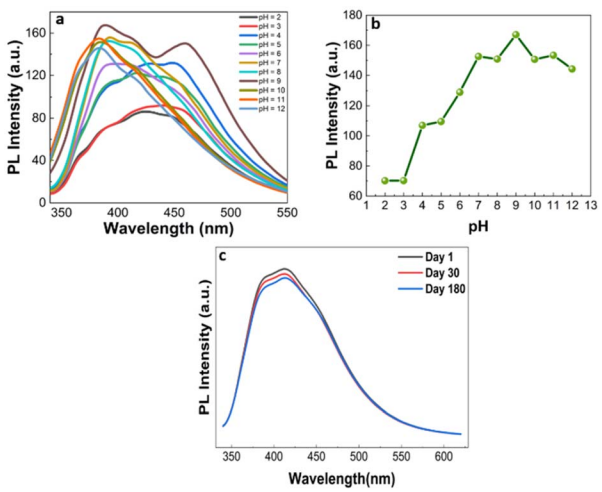

Fig. 7 (a) pH-dependent PL emissions, (b) plot of pH against PL intensity of AB-CDs respectively and (c) photostability analysis of AB-CDs at various durations of storage.

surface emissive states were not thermally disrupted.[29] The absence of noticeable thermal quenching suggests suppressed non-radiative relaxation pathways and strong surface passivation.[30] This thermal robustness confirms that AB-CDs are reliable fluorescent probes for sensing applications under elevated temperature conditions.

3.3 Detection of cholesterol

The PL properties of the aqueous AB-CDs dispersion in the presence of various biomolecules such as thiamine, L-ascorbic Acid (AA), dopamine (DA), cholesterol, L-tryptophan, D-glucose, creatinine, L-glycine, L-lycine, and L-tyrosine were investigated under identical conditions. The PL enhancement of AB-CDs (52.8% enhancement upon adding 10 μL of 1 mM cholesterol) is highly selective to cholesterol (Fig. 8). From this analysis, AB-CDs were found to be a fluorescence-based sensor, capable of selectively sensing cholesterol. The observed PL enhancement selectively for cholesterol is due to the interactions between the cholesterol and oxygen containing functionalities of AB-CDs.[31] The insignificant variation in PL intensities upon addition of different biomolecules demonstrates the potential of AB-CDs as a selective fluoroprobe for cholesterol detection.

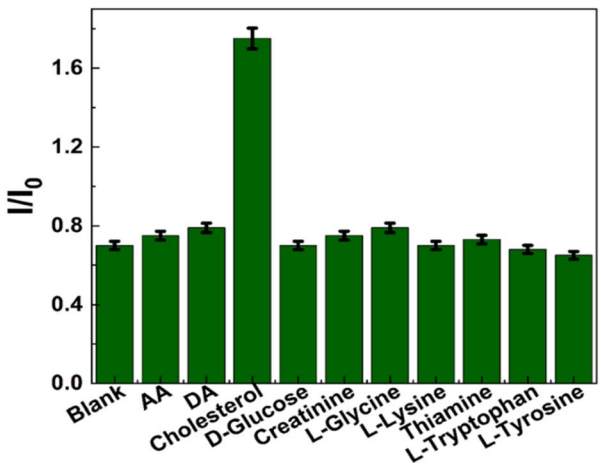

Fig. 8 Fluorescence response of AB-CDs to different biomolecules. I and I_0 represent the PL intensities at 380 nm (λ_{ex} = 320 nm) with and without biomolecules, (error amount, 3%; Y error bar of both [±] deviation).

Fig. 9a depicts fluorescence enhancement response of AB-CDs dispersion with increasing cholesterol concentrations from 0 to 8 μM. The fluorescence intensity of AB-CDs at lower cholesterol concentrations signifies the sensitivity of AB-CDs. The fluorescence enhancement showed a linear relationship between (I/I_0) and the concentration of cholesterol (I and I_0 represents AB-CDs fluorescence intensity in the presence of cholesterol and in the absence of cholesterol). A linear correlation between I/I_0 and cholesterol concentration was observed (R^2 = 0.996), with LOD equal to 0.31 μM (Fig. 9b).

3.4 Detection of chromium(VI)

The PL properties of the aqueous AB-CDs dispersion among different metal ions including Al(III), As(III), Ca(II), Cd(II), Cr(VI), Cu(II), Fe(II), Fe(III), Hg(II), Na(I), Pb(II), and Zn(II) were investigated under similar conditions. The PL quenching of AB-CDs is selective to Cr(VI) [41.7% quenching was observed upon addition of 20 μL of 1 mM of Cr(VI)] (Fig. 10). Fluorescence quenching by Cr(VI) is likely caused by its interactions with the surface carboxyl groups of AB-CDs.[31] Their quenching response for other heavy metals was not significant comparing the fluorescence intensity of AB-CDs upon adding Cr(VI), confirming their potential as fluoroprobe for detection of Cr(VI).[32]

Although some metal ions show partial quenching effects, to examine the influence of other ions in Cr(VI) detection, interference studies were carried out in the presence of coexisting metal ions (Fig. S3, SI). PL measurements were carried out using AB-CDs in the presence of a selected group of metal ions, both in the absence and presence of Cr(VI) ions (Fig. S3a, SI). In addition, fluorescence responses were evaluated for AB-CDs exposed to various metal ions along with Cr(VI) ions, and AB-CDs in the presence of Cr(VI) ions alone (Fig. S3b, SI). The

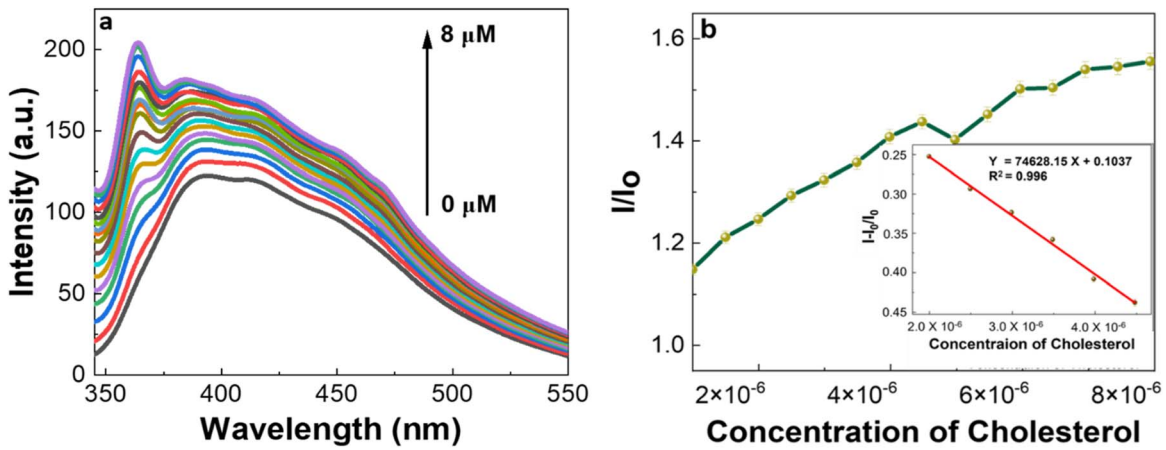

Fig. 9 (a) Fluorescence enhancement behaviour of AB-CDs dispersions to varied cholesterol concentrations at 380 nm, λ_{ex} = 320 nm, and (b) variation of I/I_0 with cholesterol concentration, with the inset showing the linear fitting at lower concentration ranges, (error amount, 3%; Y error bar of both [±] deviation).

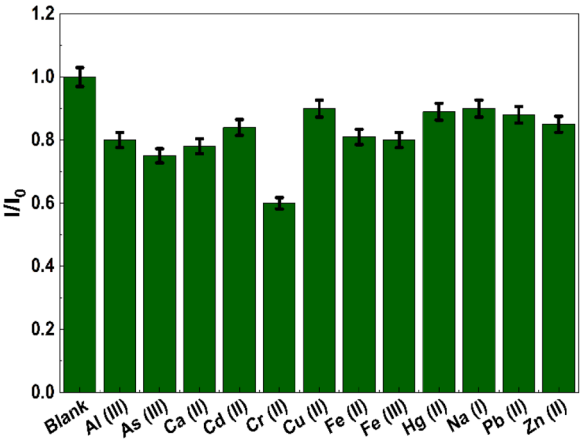

Fig. 10 Fluorescence response of AB-CDs among different ions. I represent the PL intensity with metal ions and I_0 represents PL intensities without metal ions at 415 nm (λ_{ex} = 320 nm), (error amount, 3%; Y error bar of both [±] deviation).

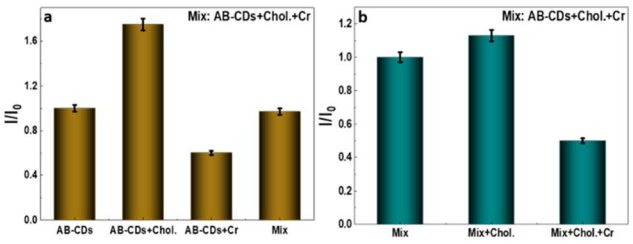

Fig. 12 (a) PL response of AB-CDs, AB-CDs in the presence of cholesterol, AB-CDs in the presence of Cr(VI) and AB-CDs to a mixture of cholesterol and Cr(VI) (Mix), and (b) PL response of Mix, cholesterol added to Mix and both cholesterol and Cr(VI) added to Mix, (error amount, 3%; Y error bar of both [±] deviation).

results from both experiments clearly demonstrate that the observed fluorescence quenching originates specifically from Cr(VI) ions. These findings further confirm the selective interaction between AB-CDs and Cr(VI), highlighting their suitability as an efficient fluorescent probe.

Fig. 11a shows fluorescence spectra of aqueous AB-CD dispersions with Cr(VI) concentrations ranging from 0 to 50 μM. AB-CD's sensitivity for Cr(VI) is revealed by the fluorescence quenching response of AB-CDs dispersions at low concentrations. A linear correlation between I/I_0 and Cr(VI) concentration was observed (R^2 = 0.995), with the limit of detection of 1.71 μM, as determined using the Stern–Volmer equation[27] (Fig. 11b).

The PL responses of the aqueous AB-CDs dispersion in the presence of cholesterol, Cr(VI), and their mixture (denoted as Mix) were recorded, as shown in Fig. 12. This analysis was carried out to evaluate the PL behaviour of AB-CDs when both cholesterol and Cr(VI) are present together in the analyte. As illustrated in Fig. 12a, AB-CDs exhibit a significant PL enhancement in the presence of cholesterol alone, whereas significant PL quenching is observed upon the addition of Cr(VI) ions alone. When both cholesterol and Cr(VI) coexist (Mix), the PL intensity is nearly identical to that of AB-CDs. Upon further addition of cholesterol to the Mix, a slight enhancement in PL intensity is observed, whereas subsequent addition of Cr(VI) ions results in marked PL quenching, attributed to the quenching effect of AB-CDs towards Cr(VI) ions (Fig. 12b).

3.5 Mechanism for the sensing of cholesterol and Cr(VI) by AB-CDs

To explore the interaction mechanism between AB-CDs and cholesterol, zeta potential studies were conducted, as depicted in Fig. S4 (SI). AB-CDs exhibited a negative surface charge of −24.8 mV in aqueous solution, attributed to the presence of carboxyl and other negatively charged functional groups. Upon interaction with cholesterol, the zeta potential changed to −16.3 mV, indicating a partial neutralization of surface charge due to electrostatic attraction between the negatively charged AB-CDs and positively charged cholesterol. These interactions are hypothesized to promote aggregation of AB-CDs.[33] The observed increase in the quantum yield from 1.62% to 2.54% in

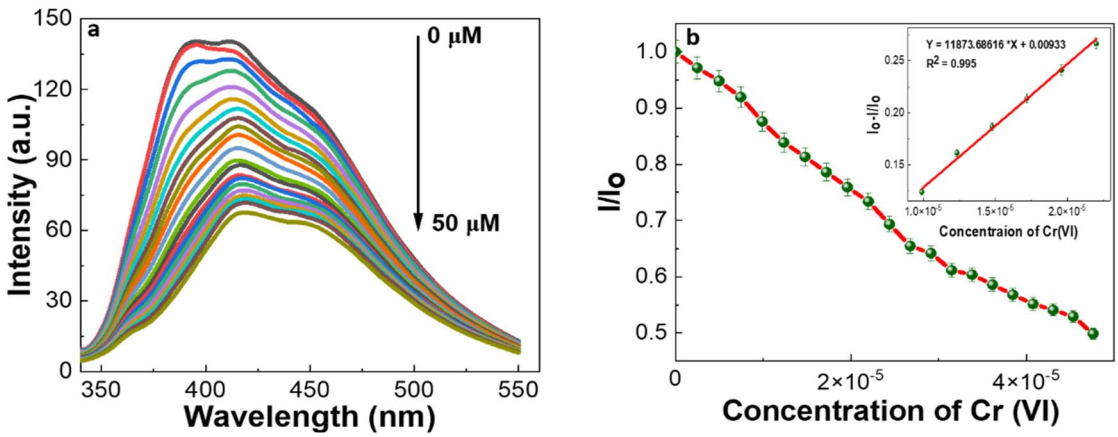

Fig. 11 (a) Fluorescence quenching behaviour of AB-CDs dispersions to varied Cr(VI) concentrations at 415 nm, λ_{ex} = 320 nm, and (b) variation of I/I_0 with Cr(VI) concentration, with the inset showing the linear fitting at lower concentration ranges, (error amount, 3%; Y error bar of both [±] deviation).

the presence of cholesterol suggests that these electrostatic interactions may promote aggregation of AB-CDs.[34] High QY in CDs arises from a combination of core structure, surface chemistry, and electronic effects that favour radiative recombination over non-radiative pathways.[35] This increased QY could potentially stabilizes the excited-state energy and thereby suppresses non-radiative decay pathways.[36] Likewise, DLS analysis revealed that the hydrodynamic diameter of AB-CDs increased nearly four-fold upon the addition of cholesterol, suggesting that AB-CDs aggregated into larger particles (Fig. S5, SI). These findings indicate that the observed fluorescence enhancement can be attributed to the higher local concentration of AB-CDs resulting from cholesterol-induced aggregation.[33] The fluorescence response of AB-CDs to cholesterol was investigated systematically. As shown in Fig. 6a, AB-CDs displayed an emission peak at 380 nm under 320 nm excitation. With increasing cholesterol concentration (0–8 μM), the fluorescence intensity at 380 nm increased significantly, while the emission peak position remained constant. This significant increase in fluorescence is proposed to result from electrostatic interactions between the negatively charged AB-CDs and the positively charged cholesterol.[37] The aggregation of AB-CDs could lead to enhanced fluorescence *via* the aggregation-induced emission (AIE) effect.[37] This enhancement appears to arises from the possible restriction of the rotational motion of surface moieties such as aromatic rings and phenolic –OH groups during aggregation.[38] Furthermore, the absorption spectra of AB-CDs before and after addition of cholesterol are presented in Fig. S6 (SI), which shows a slight decrease in absorbance on addition of cholesterol.

These results suggest a fluorescence enhancement sensing mechanism for cholesterol, which could plausibly be due to the AIE effect.[34,39]

To study the possible mechanism of quenching behaviour of AB-CDs towards Cr(VI) ions, UV-visible absorption of AB-CDs was taken and it displayed distinct peaks at 212 nm and 280 nm, corresponding to π–π* transitions of conjugated C=C bonds and n–π* transitions of C=O groups, respectively (Fig. 6a). A strong emission peak centered at 415 nm was recorded when AB-CDs were excited at 320 nm (Fig. 6b). As revealed in the PL spectra, AB-CDs exhibited excitation-dependent emission, with excitation wavelengths ranging from 220 to 260 nm (Fig. 6c). As illustrated in Fig. S7 (SI), absorption peaks of Cr(VI) were observed at 272 nm and 368 nm. Meanwhile, the excitation spectrum of AB-CDs showed bands at 236 and 323 nm, with their emission centred at 415 nm under 320 nm. This overlap of spectra between the absorption peak of Cr(VI) and excitation/emission bands of AB-CDs supports the inner filter effect[40,41] which is proposed as a potential mechanism for PL quenching of AB-CDs by Cr(VI) ions.

3.6 Comparison of the sensing performance of AB-CDs with previously reported sensing platforms for Cr(VI) and cholesterol detection

The sensing performance of AB-CDs towards Cr(VI) was compared with previously reported fluoroprobes, as detailed in Table S1 (SI). Owing to AB-CDs sustainable, renewable, eco-friendly, cost-effective, and biocompatible nature, they can serve as an effective and cheap fluorescent probe for the sensitive detection of Cr(VI) ions. Their synthesis was carried out *via* a green and straightforward method under mild conditions, thereby aligning with environmentally friendly sensor development. In contrast, the fluoroprobes listed in Table S1 (SI), were generally synthesized using synthetic precursors and organic solvents. Although the LOD of AB-CDs is relatively higher than other reported fluoroprobes, their cost-effectiveness and eco-friendly synthesis make them a promising alternative. Similarly, the sensing of cholesterol using AB-CDs was evaluated against previously reported biosensors, as summarized in Table S2 (SI). In contrast to other approaches that utilize CDs as nanozymes within multi-component and complex detection systems, AB-CDs offers a simple, green, and cost-effective alternative for rapid and sensitive sensing of cholesterol. The detection limit of cholesterol using AB-CDs was comparatively better when compared to other reported biosensors. Overall, AB-CDs served as novel fluoroprobe with excellent selectivity and sensitivity toward sensing of both cholesterol as well as Cr(VI) ions, with added advantages in terms of sustainability and simple synthesis process.

4 Conclusions

We report a green method to synthesize CDs using the *Averrhoa bilimbi*. *Averrhoa bilimbi* as a source of CDs for the multi analyte detection of Cr(VI) and cholesterol has not been reported elsewhere. The hydrothermal method utilized in this study to synthesize AB-CDs is simple and cost-effective. With an average size of 6.022 nm, the quasi-spherical particles AB-CDs exhibited emissions dependent on both pH and excitation wavelength. We developed a fluorescent sensor from AB-CDs, which is sensitive to cholesterol and Cr(VI). The detection limits of the sensor to the analytes cholesterol and chromium(VI) were calculated to be 0.31 μM and 1.71 μM, respectively. These findings demonstrate the potential of AB-CDs as an efficient, sustainable, and eco-friendly fluoroprobe for selective and sensitive detection of biologically and environmentally relevant targets, offering a promising platform for future diagnostic and environmental monitoring applications.

Author contributions

Aishwarya Joji Mathew: conceptualization, methodology, investigation, data curation, formal analysis, software, visualization, validation and writing – original draft, writing – review & editing. Varsha Lisa John: conceptualization, methodology, investigation, data curation, formal analysis, software, visualization, validation and writing – original draft. Aiswarya P. S.: conceptualization, methodology, and data curation. Vinod T. P.: conceptualization, investigation, formal analysis, software, visualization, validation, resources, writing – original draft, writing – review & editing, funding acquisition and project administration and supervision.

Conflicts of interest

The authors declare that they have no known competing financial interests or personal relationships that could have appeared to influence the work reported in this paper.

Data availability

The data supporting this article will be made available upon request.

Supplementary information (SI) is available. See DOI: https://doi.org/10.1039/d6ra00222f.

Acknowledgements

Authors acknowledge CHRIST (Deemed to be University), Bangalore, India for research facilities. Vinod T. P. is thankful to Centre for Research Projects (CRP), Christ University, for the Seed Money Grant SMSS-2334 and Vision Group on Science and Technology (VGST), Govt. of Karnataka for K-FIST-L1 grant (GRD No. 1143).

References

1 V. Lisa John, F. Joy, A. Jose Kollannoor, K. Joseph, Y. Nair and T. P. Vinod, *J. Colloid Interface Sci.*, 2022, **617**, 730–744.
2 X. Xu, R. Ray, Y. Gu, H. J. Ploehn, L. Gearheart, K. Raker and W. A. Scrivens, *J. Am. Chem. Soc.*, 2004, **126**, 12736–12737.
3 S. A. Shaik, S. Sengupta, R. S. Varma, M. B. Gawande and A. Goswami, *ACS Sustain. Chem. Eng.*, 2021, **9**, 3–49.
4 P. Zhu, X. Zhao, Q. Zhu, X. Han, Y. Tang, S. Liao, Z. Guo, Z. Wang, W. Bi, Q. Xu, L. Zhang and M. Xu, *Chem. Eng. J.*, 2023, **470**, 144042.
5 V. L. John, A. R. Nayana, T. R. Keerthi, K. A. Athira Krishnan, B. C. P. Sasidharan and T. P. Vinod, *Macromol. Biosci.*, 2023, **23**, 2300081.
6 M. Hamed, S. Chinnam, A. Bedair, S. Emara and F. R. Mansour, *Talanta Open*, 2024, **10**, 100348.
7 J. Fan, L. Kang, X. Cheng, D. Liu and S. Zhang, *Nanomaterials*, 2022, **12**, 4473.
8 S. Priya and S. R. Suseem, *Nano Express*, 2024, **5**, 012002.
9 Y. Tang, Q. Xu, X. Zhang, R. Zhu, N. Zhao and J. Wang, *Nano Res.*, 2024, **17**, 10109–10118.
10 G. Ayiloor Rajesh, V. L. John, A. Pookunnath Santhosh, A. Krishnan Nair Ambika and V. Thavarool Puthiyedath, *Part. Part. Syst. Charact.*, 2022, **39**, 2200017.
11 T. Anusuya, V. Kumar and V. Kumar, *Chemosphere*, 2021, **282**, 131019.
12 Q. Luo, X. Huang, Y. Luo, H. Yuan, T. Ren, X. Li, D. Xu, X. Guo and Y. Wu, *Chem. Eng. J.*, 2021, **407**, 127050.
13 Q. Huang, Q. Bao, C. Wu, M. Hu, Y. Chen, L. Wang and W. Chen, *J. Pharm. Anal.*, 2022, **12**, 104–112.
14 P. Krishnaiah, R. Atchudan, S. Perumal, E.-S. Salama, Y. R. Lee and B.-H. Jeon, *Chemosphere*, 2022, **286**, 131764.
15 R. N. C. S. Carvalho, G. B. Brito, M. G. A. Korn, J. S. R. Teixeira, F. de S. Dias, A. F. Dantas and L. S. G. Teixeira, *Anal. Methods*, 2015, **7**, 8714–8719.
16 H. Zhang, Y. Chen, M. Liang, L. Xu, S. Qi, H. Chen and X. Chen, *Anal. Chem.*, 2014, **86**, 9846–9852.
17 T. T. Bui and S.-Y. Park, *Green Chem.*, 2016, **18**, 4245–4253.
18 Y. Chen, G. Yang, S. Gao, L. Zhang, M. Yu, C. Song and Y. Lu, *RSC Adv.*, 2020, **10**, 39596–39600.
19 P. Das, S. Ganguly, P. P. Maity, M. Bose, S. Mondal, S. Dhara, A. K. Das, S. Banerjee and N. C. Das, *J. Photochem. Photobiol. B Biol.*, 2018, **180**, 56–67.
20 K. G. Nguyen, I.-A. Baragau, R. Gromicova, A. Nicolaev, S. A. J. Thomson, A. Rennie, N. P. Power, M. T. Sajjad and S. Kellici, *Sci. Rep.*, 2022, **12**, 13806.
21 P. Pansari, G. Durga and R. Javed, *Chem. Pap.*, 2024, **78**, 5993–6010.
22 L. M. Malard, M. A. Pimenta, G. Dresselhaus and M. S. Dresselhaus, *Phys. Rep.*, 2009, **473**, 51–87.
23 J. Ge, Q. Jia, W. Liu, M. Lan, B. Zhou, L. Guo, H. Zhou, H. Zhang, Y. Wang, Y. Gu, X. Meng and P. Wang, *Adv. Healthcare Mater.*, 2016, **5**, 665–675.
24 J. Kim, H. J. Shim, J. Yang, M. K. Choi, D. C. Kim, J. Kim, T. Hyeon and D. Kim, *Adv. Mater.*, 2017, **29**, 1700217.
25 S. Sahu, B. Behera, T. K. Maiti and S. Mohapatra, *Chem. Commun.*, 2012, **48**, 8835.
26 Z. Gan, H. Xu and Y. Hao, *Nanoscale*, 2016, **8**, 7794–7807.
27 V. Lisa John, F. P M, C. K P and V. T P, *Nanotechnology*, 2022, **33**, 495706.
28 D. Tatini, A. Fidi, M. Acar and P. Lo Nostro, *Colloids Surf., AC*, 2026, **736**, 139621.
29 S. Priya, E. Karthikeyan, C. P. Reshmi, P. D. Raju, C. V. Suneesh, K. Sandeep and A. R. Ramesh, *RSC Adv.*, 2025, **15**, 50001–50009.
30 Q. Zhang, M. He, Q. Wan, W. Zheng, M. Liu, C. Zhang, X. Liao, W. Zhan, L. Kong, X. Guo and L. Li, *Chem. Sci.*, 2022, **13**, 3719–3727.
31 S. Zhuo, Y. Guan, H. Li, J. Fang, P. Zhang, J. Du and C. Zhu, *Analyst*, 2019, **144**, 656–662.
32 S. Bhatt, M. Bhatt, A. Kumar, G. Vyas, T. Gajaria and P. Paul, *Colloids Surf., B*, 2018, **167**, 126–133.
33 J. Guo, W. Lu, Y. Meng, Y. Liu, C. Dong and S. Shuang, *Analyst*, 2022, **147**, 5455–5461.
34 S. A. Fatah and K. M. Omer, *Microchem. J.*, 2025, **214**, 114094.
35 S. Zhu, Y. Song, J. Wang, H. Wan, Y. Zhang, Y. Ning and B. Yang, *Nano Today*, 2017, **13**, 10–14.
36 K. Nandhini and M. Ilanchelian, *J. Fluoresc.*, 2025, **35**, 11261–11271.
37 L. Li, L. Shi, J. Jia, O. Eltayeb, W. Lu, Y. Tang, C. Dong and S. Shuang, *Sens. Actuators, B*, 2021, **332**, 129513.
38 S. Pawar, S. Kaja and A. Nag, *ACS Omega*, 2020, **5**, 8362–8372.
39 V. Bavya, T. P. D. Rajan and K. I. Suresh, *Langmuir*, 2025, **41**, 1333–1343.
40 M. Zheng, Z. Xie, D. Qu, D. Li, P. Du, X. Jing and Z. Sun, *ACS Appl. Mater. Interfaces*, 2013, **5**, 13242–13247.
41 A. J. Mathew, T. P. Vinod and Y. Nair, *Nanoscale Adv.*, 2025, **7**, 7836–7848.